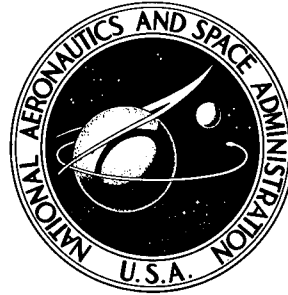


SK1
ADD4 22104

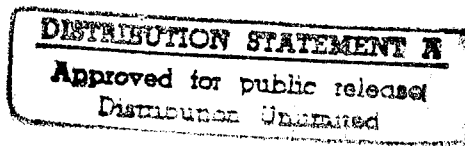
NASA TECHNICAL NOTE



NASA TN D-8411

NASA TN D-8411

19960306 058



DEPARTMENT OF DEFENSE
TECHNICAL EVALUATION CENTER
PICATINNY ARSENAL, DOVER, N. J.

EFFECT OF LOW-VELOCITY IMPACT DAMAGE ON THE COMPRESSIVE STRENGTH OF GRAPHITE-EPOXY HAT-STIFFENED PANELS

*Marvin D. Rhodes, Jerry G. Williams,
and James H. Starnes, Jr.*

*Langley Research Center
Hampton, Va. 23665*

DTIC QUALITY INSPECTED 1

NATIONAL AERONAUTICS AND SPACE ADMINISTRATION • WASHINGTON, D. C. • APRIL 1977

PLASTEC 25406

CONTENTS

SUMMARY	1
INTRODUCTION	1
DESIGN AND FABRICATION OF TEST SPECIMENS	2
Specimen Design	3
Design A	3
Design B	3
Specimen Fabrication	3
APPARATUS	4
TESTS	4
Control Tests	4
Undamaged panels	4
Panel with a cutout	4
Impact-Damage Tests	5
RESULTS AND DISCUSSION	5
Control Tests	5
Undamaged panels	5
Panel with a cutout	5
Impact Damaged Panels	6
Impact damage in the high-axial-stiffness region	6
Low axial strain at impact	6
High axial strain at impact	7
Impact-damage characterization	8
Impact damage in the low-axial-stiffness region	9
CONCLUDING REMARKS	9
REFERENCES	11
TABLES	12
FIGURES	14

1. Report No. NASA TN D-8411		2. Government Accession No.		3. Recipient's Catalog No.	
4. Title and Subtitle EFFECT OF LOW-VELOCITY IMPACT DAMAGE ON THE COMPRESSIVE STRENGTH OF GRAPHITE-EPOXY HAT-STIFFENED PANELS				5. Report Date April 1977	
				6. Performing Organization Code	
7. Author(s) Marvin D. Rhodes, Jerry G. Williams, and James H. Starnes, Jr.				8. Performing Organization Report No. L-11222	
9. Performing Organization Name and Address NASA Langley Research Center Hampton, VA 23665				10. Work Unit No. 505-02-42-01	
				11. Contract or Grant No.	
12. Sponsoring Agency Name and Address National Aeronautics and Space Administration Washington, DC 20546				13. Type of Report and Period Covered Technical Note	
				14. Sponsoring Agency Code	
15. Supplementary Notes					
16. Abstract <p>An experimental investigation was conducted to determine the effect of low-velocity impact damage on the compressive strength of graphite-epoxy hat-stiffened panels. Fourteen panels, representative of minimum-mass designs for two compression load levels (0.53 MN/m (3000 lbf/in.) and 1.58 MN/m (9000 lbf/in.)), were tested. Eight panels were damaged by impact and the effect on compressive strength was evaluated by comparing the results with data for control panels. The impact tests consisted of firing 1.27-cm-diameter aluminum projectiles normal to the plane of the panel at a velocity of approximately 55 m/s to simulate impact damage from runway debris.</p> <p>The results of this investigation indicate that the extent of damage in the high-axial-stiffness region of both panel designs increased with the magnitude of applied axial load. The damage in panels designed for 0.53 MN/m at a strain of 0.0034 was local and the damaged panels were capable of carrying the design load. The panels designed for 1.58 MN/m at a strain of 0.0080, however, failed due to impact damage at applied axial strains 50 to 58 percent of the design level. The existence of, and not necessarily the extent of, damage in the high-axial-stiffness region was the most significant factor in reducing panel strength. Limited damage that was not visually detectable reduced ultimate strength as much as extensive visible damage.</p>					
17. Key Words (Suggested by Author(s)) Impact damage Graphite epoxy Stiffened panels Effect of cutouts Compression panels Panel buckling Delamination				18. Distribution Statement Unclassified - Unlimited Subject Category 39	
19. Security Classif. (of this report) Unclassified		20. Security Classif. (of this page) Unclassified		21. No. of Pages 28	
				22. Price* \$4.00	

EFFECT OF LOW-VELOCITY IMPACT DAMAGE ON THE COMPRESSIVE STRENGTH OF GRAPHITE-EPOXY HAT-STIFFENED PANELS

Marvin D. Rhodes, Jerry G. Williams,
and James H. Starnes, Jr.
Langley Research Center

SUMMARY

An experimental investigation was conducted to determine the effect of low-velocity impact damage on the compressive strength of graphite-epoxy hat-stiffened panels. Fourteen panels, representative of minimum-mass designs for two compression load levels (0.53 MN/m (3000 lbf/in.) and 1.58 MN/m (9000 lbf/in.)), were tested. Eight panels were damaged by impact and the effect on compressive strength was evaluated by comparing the results with data for control panels. The impact tests consisted of firing 1.27-cm-diameter aluminum projectiles normal to the plane of the panel at a velocity of approximately 55 m/s to simulate impact damage from runway debris.

The results of this investigation indicate that the extent of damage in the high-axial-stiffness region of both panel designs increased with the magnitude of applied axial load. The damage in panels designed for 0.53 MN/m at a strain of 0.0034 was local and the damaged panels were capable of carrying the design load. The panels designed for 1.58 MN/m at a strain of 0.0080, however, failed due to impact damage at applied axial strains 50 to 58 percent of the design level. The existence of, and not necessarily the extent of, damage in the high-axial-stiffness region was the most significant factor in reducing panel strength. Limited damage that was not visually detectable reduced ultimate strength as much as extensive visible damage.

INTRODUCTION

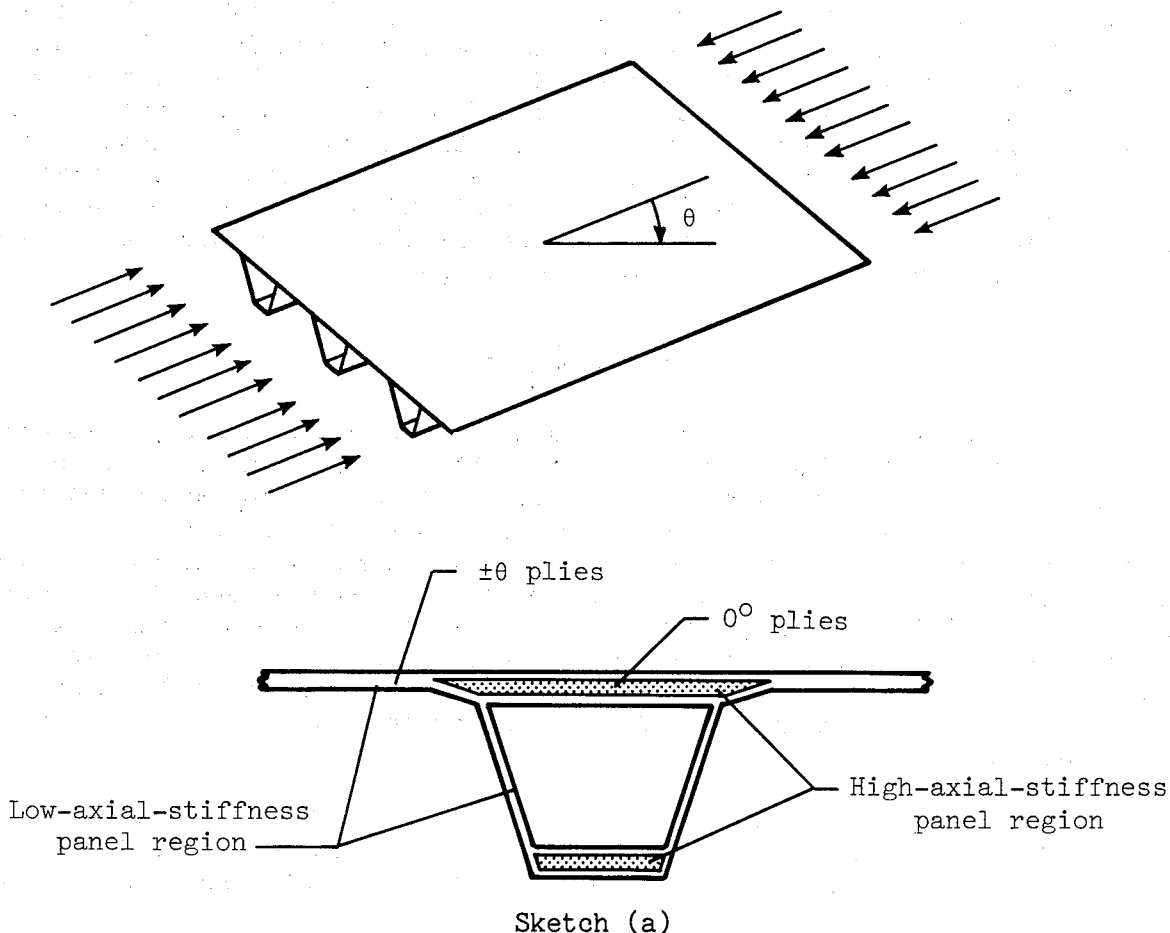
The most efficient hat-stiffened graphite-epoxy compression panels have been shown to be approximately 50 percent lighter than the most efficient stiffened aluminum compression panels (refs. 1 and 2). This mass reduction makes graphite-epoxy panels attractive candidates for aircraft applications, but before they can be used in commercial service certain operational hazards must be considered. Aircraft can be subjected to impact damage, for example, and the effects of such damage must be established. Low-velocity impact damage has been shown to cause significant reductions in the load-carrying capability of some thin, honeycomb-stabilized, graphite-epoxy laminates (refs. 3 and 4). The effect of impact damage on stiffened compression panels, however, has not been assessed.

This paper presents the results of an exploratory test program to determine the effect of low-velocity impact damage on minimum-mass hat-stiffened compression panels. The panels were designed for two different compression

loads (0.53 MN/m (3000 lbf/in.) and 1.58 MN/m (9000 lbf/in.)) with buckling as the primary design constraint. The test results presented include data for control panels (undamaged panels and a panel with a 1.27-cm-diameter cutout) and data for impact-damaged panels. The undamaged panels were used to verify the design and establish critical strain levels for compression loading. The panel with the 1.27-cm-diameter cutout, which simulated local damage, provided comparative data for a panel with a well-defined flaw. The impact-damaged panels were used to determine the effect of this type of damage for a range of applied strain. These panels were subjected to impact while under load to evaluate the effect of applied strain on local damage, and some were subsequently loaded to evaluate residual strength.

DESIGN AND FABRICATION OF TEST SPECIMENS

Two different designs (A and B) of highly efficient hat-stiffened panels with minimum-mass proportions were tested in this investigation. Design A was critical in buckling at a load of 0.53 MN/m, which corresponds to an axial strain of 0.0034. Design B was more heavily loaded (1.58 MN/m) and was critical in buckling at a strain of 0.008. Buckling was regarded as failure for design purposes in both design A and design B. The basic configuration for both hat-stiffened-panel designs is shown schematically in the following sketch:



Specimen Design

Panels were designed using a minimum-mass synthesis computer program that includes buckling and strength constraints (ref. 5). The elastic material properties used in panel designs are given in table I. The buckling constraints accounted for simply supported wide-column Euler buckling as well as local buckling, that is, short-wavelength panel buckling of the skin, stiffener caps, and webs. The bending stiffness required for wide-column Euler buckling is primarily provided by the high-axial-stiffness regions in the cap of the hat and in the skin beneath the hat which contain 0° plies. (See sketch (a).) The webs and the skin between stiffeners have low axial stiffness and consist entirely of angle ($\pm\theta$) plies. (See sketch (a).) The critical Euler-buckling design length for both panel types is 76.2 cm. Specimens tested in this investigation were 43.7 cm or less in length and, therefore, were critical in local buckling.

Design A.— Details of the cross section of the panels designed to carry a load of 0.53 MN/m are presented in figure 1(a). At this design load the panels had an imposed axial strain of 0.0034. The angle plies in the webs and skin were oriented at $\pm 52^\circ$. The final design mass per unit area was 3.56 kg/m² (0.73 lbm/ft²). Both three-stiffener-wide and four-stiffener-wide panels were tested in this investigation. Test panel dimensions (panels A1 to A5) are given in table II.

Design B.— Details of the cross section of the panels designed to carry a load of 1.58 MN/m are presented in figure 1(b). At this design load the panels had an imposed axial strain of 0.0080. The angle plies in the webs and skin were oriented at $\pm 45^\circ$. The panel design mass per unit area was 6.10 kg/m² (1.25 lbm/ft²). Both two-stiffener-wide and three-stiffener-wide panels were tested in this investigation. Test panel dimensions (panels B1 to B9) are given in table II.

Specimen Fabrication

The specimens tested in this investigation were fabricated from 7.6-cm-wide preimpregnated tape of Thornel 300 graphite in Narmco 5208 epoxy resin. The resin is a 450-K curing system and the tape has a nominal cured thickness of 0.14 mm per ply. The specimens were manufactured using an aluminum tool which was machined with the required hat-stiffener-design cross-sectional dimensions. The angle and 0° plies for the stiffeners were laid in the mold. Premolded trapezoidal-shaped rubber inserts were positioned in the mold and the skin plies were laid on top. The panel was covered by an aluminum caul plate and the entire assembly was bagged and cured in an autoclave. The cured specimens were then trimmed, and the ends were potted in an epoxy resin and ground flat and parallel for uniform compression loading. Detail design considerations, analysis methods, and manufacturing procedures are described in references 1 and 2.

APPARATUS

The test specimens were loaded in axial compression using a hydraulic testing machine with a 1.33-MN capacity. Electrical resistance strain gages were used to monitor panel strains. A direct-current-differential transformer (DCDT) was used to monitor displacements normal to the surface of the panels. Strains, displacements, and loads were recorded on magnetic tape and selected gages were monitored during the test on an oscilloscope. The moiré-fringe method for observing lateral displacements was used to monitor buckle patterns and delamination growth during loading. The basic instrumentation for this purpose included a high-intensity light source, a grid pattern of 20 lines per centimeter mounted on a transparent plastic sheet held near the specimen, and a camera to record photographically the fringe pattern at selected loads.

The equipment used to propel the impact projectile is shown schematically in figure 2. Air pressure developed in the reservoir ruptures the diaphragm. The high-pressure air passes through an orifice and forces the projectile down the barrel. An electronic detector located at the muzzle of the barrel is used to measure the velocity of the projectile. The test panels were placed within 25 cm of the gun muzzle.

Several panels with impact damage were examined with an ultrasonic flaw detector. The detector was a focused pulse-echo type, high-resolution commercial instrument which used a 15-MHz piezoelectric transducer. The transducer and panels were immersed in a tank of water to provide a medium for the ultrasonic transmission, and the transducer was mounted to a traversing mechanism which automatically scanned the region of interest. The scan was synchronized with an oscilloscope for purposes of recording data. Additional information concerning this equipment and procedure can be found in reference 6.

TESTS

Tests were conducted on undamaged panels and on one panel with a circular cutout to provide control data for comparison with the impact-damage tests. Loading conditions and impact location for each panel tested are given in table II.

Control Tests

Undamaged panels.— Several undamaged panels were tested in compression to determine the critical load and strain at which local buckling occurred. Local buckling was defined using the load/strain response and strain-reversal techniques. The strain measurements were complemented by the moiré-fringe method which provided visual definition of the buckled-mode shape.

Panel with a cutout.— A hat-stiffened panel with a 1.27-cm-diameter circular hole was loaded in compression to evaluate the effect of a well-defined damaged area on panel performance. The hole was located in the high-axial-stiffened region beneath the cap in the middle of the center stiffener. It was drilled using a diamond impregnated core bit. The panel was instrumented

with approximately 40 strain gages and loaded to failure. Displacements normal to the surface in the center of the panel were measured with a DCDT. The strain measurements were complemented by the moiré-fringe method which provided visual definition of the buckled-mode shape.

Impact-Damage Tests

Several panels were damaged by impact in the high-axial-stiffness region while under compression load to evaluate the effect of load on impact-initiated damage. The panels were then taken to higher loads to evaluate the effect of damage on buckling and residual strength. One panel was also damaged by impact in the low-axial-stiffness region in the skin between stiffeners. Aluminum spheres 1.27 cm in diameter were used as the impact projectile. Aluminum was chosen as the projectile material because it has about the same density as common rock materials and is therefore representative of runway debris. The projectile impacts were normal to the panel surface at a velocity of about 55 m/s.

RESULTS AND DISCUSSION

Control Tests

Undamaged panels.— Three panels of design A and four of design B were tested in the undamaged condition to evaluate panel behavior due to applied axial compressive load. The response of each panel to the indicated applied load, or strain, is presented in table II. The design A panels buckled near the design strain of 0.0034 and exhibited postbuckling behavior. The design B panels exhibited strength failure near the design strain of 0.0080 prior to buckling. Photographs of a typical normal displacement field as indicated by the moiré-fringe pattern for both design configurations are shown in figure 3. Test panel A1 (fig. 3(a)) has a fully developed buckle pattern at an imposed strain of 0.0036. Test panel B2 (fig. 3(b)) is shown at an imposed axial strain of 0.0079 which is near the strain at which the panel exhibited failure. The pattern seen at the ends of the panel is the result of in-plane restraints imposed by the flat-end test condition (ref. 2).

Panel with a cutout.— Panel B5 with the 1.27-cm-diameter cutout was loaded to failure in axial compression. Far-field axial strains were measured during the test by five strain gages located on a line across the panel, 6.35 cm from the cutout center. The locations of those gages and the strains as a function of load are shown in figure 4. These data indicate a nearly uniform far-field axial strain distribution across the panel and a linear load-strain relationship to failure. The average of these gages is referred to in this paper as the applied strain. Panel failure occurred at an applied strain of 0.0058 (applied load of 496 kN) which is 73 percent of the 0.0080 design strain.

Several strain gages were located at points along a line across the panel passing through the cutout center to determine the variation in axial strain in the neighborhood of the cutout. These gages were closely spaced near the

cutout and one gage was located on the cutout free-edge surface. The distribution of strain as determined by these gages across the right side of the panel normalized by the applied strain is shown in figure 5. The strains are several times greater near the cutout edge than those 3 cutout radii away and there are steep strain gradients near the cutout edge. Up to an applied strain of about 0.0034 the strain at the cutout edge is approximately 4.6 times greater than the far-field strain. At an applied strain of 0.0034 the strain at the cutout edge was initially 0.016 and then dropped suddenly to 0.012. It is suspected that a local material failure occurred at this very high strain level. At applied strains between 0.0034 and 0.0049 the strains at the cutout edge were only 2.4 to 2.8 times as great as the far-field strains as indicated by the results shown in figure 5.

At applied strains near 0.0049 large changes in strain were recorded near the cutout and noticeable panel displacements began to develop in the vicinity of the cutout. Moiré-fringe patterns representing the normal displacement field near the cutout are shown in figure 6 for several values of applied strain. A representative moiré-fringe pattern for an applied strain of 0.0048 is shown in figure 6(a) and a closeup of the cutout region for this applied strain is shown in figure 6(b). At an applied strain of approximately 0.0049 a local buckling displacement field began to develop at the cutout edge about 60° counterclockwise from the loading axis. This displacement field was about 1.0 cm long for an applied strain of 0.0050 and is shown in figure 6(c). As the applied strain was increased, the extent of the displacement field increased to a length of about 1.8 cm for an applied strain of 0.0055 as shown in figure 6(d). At an applied strain of 0.0057, the displacement field had rotated counterclockwise to a position 90° from the loading axis (fig. 6(e)) and extended on both sides of the cutout. This displacement field extended about 2.5 cm on the left side and about 2.4 cm on the right side of the cutout which makes the total length of this displacement field approximately equal to the width of the 0° fibers in the skin under the stiffener. The local displacement field propagated across the panel (fig. 6(f)) at an applied strain of 0.0058 which indicates that the local behavior precipitated panel failure.

Impact Damaged Panels

Impact damage in the high-axial-stiffness region.- Several panels were damaged by impact in the high-axial-stiffness region while subjected to applied axial compression strain.

Low axial strain at impact: Test panels A4, A5, and B6 were damaged by impact after a small axial load was applied. (See table II.) A visual examination of the area where impact occurred revealed no apparent local damage. All three specimens were subsequently loaded to failure. Several strain gages away from the impact region were used to monitor the applied axial strains. The average of these gages is referred to in this paper as the applied strain. The applied strain at failure for all three test panels is given in table II.

Photographs of the moiré-fringe pattern of panel A4 loaded prior to failure and of the failed panel are shown in figure 7. The moiré-fringe pattern (fig. 7(a)) is similar to that of the undamaged panel A1 (fig. 3(a)). The dark

spot in the center of the panel is the impact location where the paint has been removed for post impact inspection. Figure 7(b) indicates that the panel failure region is extensive and includes the impact location. The panel was inspected ultrasonically prior to failure, and a photograph of the oscilloscope record for the region in the vicinity of the impact location is shown in the insert of figure 7(a). The area represented by the insert is outlined on the photograph. The dark area shown in the insert indicates subsurface damage in the panel. This area is about 6.35 cm long and about as wide as the region beneath the hat which contains 0° plies. The results of tests on panels A4 and A5 were similar and both panels failed at applied strains near their design strain level (0.0034).

Photographs of the moiré-fringe pattern prior to failure and of the failed panel B6 are shown in figure 8. A small circular pattern in the region of impact was observed with the moiré-fringe technique indicating the presence of local damage. The development of this fringe pattern and an examination of the panel failure indicate that the impact damage precipitated the panel failure. Failure occurred at an applied strain of 0.0043 which is about 54 percent of the design value.

Two stiffener sections, typical of those of panel B6, were damaged by impact at zero applied axial strain and ultrasonically inspected. Identical results were obtained for these two sections. A photographic record of the ultrasonic inspection is shown in the insert of figure 8(a). The subsurface-damage region is oval shaped and is about 2.54 cm wide by 3.81 cm long. One of the stiffeners was cross-sectioned in the region of impact damage and examined microscopically. A photomicrograph of the cross section at a low level of magnification is shown in figure 9. This photomicrograph reveals delamination in the cross section with the most severe delamination occurring on the back surface of the laminate. Striations or hairline crack patterns through the thickness can also be observed. These cracks converge on the point of impact and are similar to those patterns observed for impact-damaged glass panels. Both the cracking and the delamination are probably the result of stress waves generated by the projectile impact.

High axial strain at impact: Test panels A3, B7, and B8 were damaged by impact with a high axial load applied. (See table II.) Panels A3 and B7 which had an applied axial strain of 0.0034 and 0.0030, respectively, had a large region of visually detectable damage in the impact area. Instrumentation monitoring applied load indicated both panels had significant load reductions at impact due to loss in panel stiffness (table II). Both were subsequently loaded to failure to determine the panel residual strength. Panel A3 was ultrasonically inspected prior to the residual strength test and an extensive region of subsurface damage was detected. A photograph of the moiré-fringe pattern of the panel loaded prior to failure is shown in figure 10(a) where the subsurface-damage region is outlined. Even though the damage in panel A3 is extensive, it buckled at an applied strain near the design level and carried additional load after buckling similar to the undamaged panels. The panel failed in the region of the impact damage (fig. 10(b)) at an applied strain of 0.0037. Comparison of panel A3 with panels A4 and A5, all of which were designed for a load of 0.53 MN/m at an axial strain of 0.0034, indicates that

the extent of the subsurface damage did not significantly affect the strain level at which the panels failed.

Several photographs of the moiré-fringe pattern taken during the residual strength test of panel B7 are shown in figure 11 along with a photograph of the failed panel. The moiré-fringe pattern shows considerable lateral deformation of the panel center, which may be due to impact-induced delamination or skin buckling. When the panel was damaged by impact, a reduction in applied load of 28.9 kN was measured. The 28.9-kN load reduction approximately corresponds to the load which the high-axial-stiffness region beneath the center stiffener is calculated to carry for an imposed strain of 0.0030. The panel failed at an applied strain of 0.0046 which is 58 percent of the design value.

Panel B8 had an applied axial strain of 0.0040 (50 percent of design strain) and failed catastrophically on impact. The failure was similar to the ultimate failure of panel B7. After failure the panel was cross-sectioned and examined with a microscope. This examination revealed considerable interior damage in the laminate near the impact location. Cracking similar to that previously discussed was also observed. The combination of applied axial load and dynamic stress waves generated by the projectile impact forms a complicated three-dimensional stress field in the orthotropic laminates of these test panels. This situation suggests that a simple criterion may not be adequate to predict panel failure.

Impact-damage characterization: A comparison of test results for impact damage in the high-axial-stiffness region indicates both similarities and differences in the results for panels of design A and design B. The extent of local damage induced by impact increased with the magnitude of applied axial-compression strain for both designs. The design A panels satisfied the design-strain requirements with the presence of impact damage and also exhibited post-buckling behavior. The design B panels, however, failed due to impact damage at applied axial strains between 50 and 58 percent of the design strain level. Failure strains for impact-damaged panels and the control panel with circular cutout can be compared in figure 12. Limited local impact damage that was not noticeable by visual inspection (panel B6) reduced the ultimate strength of the design B panels as much as extensive visible localized damage (panel B7). All three of the design B panels damaged by impact failed at lower applied strain levels than the control test panel with the 1.27-cm-diameter cutout. The damaged region caused by impact, however, was larger than the cutout. For all design B panels the damage in the high-axial-stiffness region precipitated failure at an applied strain well below the design strain level.

The results of this investigation suggest that impact causes considerable delamination, and examination of the panel cross section showed that the delamination occurred primarily at the interface between the 0° and 45° plies (fig. 9). The discrete layers formed by delamination may not be midplane symmetric and, therefore, exhibit anisotropic coupling effects. The boundaries of these discrete layers are highly irregular (fig. 10) and are subjected to high interlaminar normal and shear stresses. Also, delamination reduces the local cross-sectional bending stiffness and causes locally eccentric loading which introduces transverse shear forces and moments not present in the undamaged panel. These local eccentric forces and anisotropic effects cause

local deformations and strain gradients to occur in the delaminated region that could be sufficient to make local geometric- and material-property nonlinearities important factors. Since these eccentrically loaded layers are thinner and less stiff than the undamaged laminate, they can buckle locally at a lower load than the undamaged laminate. This buckling could cause a local load redistribution in the panel that, in turn, could cause the damage to propagate and the panel to fail. The results of this investigation suggest that highly efficient graphite-epoxy hat-stiffened compression panels designed for high strain (0.0080) can exhibit serious degradation due to impact damage; however, efficient damage-tolerant designs can be obtained for more moderate design strains.

Impact damage in the low-axial-stiffness region.- In order to evaluate the effect of damage in the angle-ply, low-axial-stiffness region, panel B9 was damaged by impact in the skin region between stiffeners ($\pm 45^\circ$ for the design B panels). The panel was loaded to an applied axial strain of 0.0040 when impact occurred. (See table II.) No reduction in the applied load upon impact was observed and no increase in axial strain was noted in the gage near the point of impact. Although some local fiber failure and delamination was observed, the failure did not propagate. After impact the panel was loaded to an applied strain of 0.0054 without propagation of local damage. At this load the panel was damaged in the remaining $\pm 45^\circ$ skin region between stiffeners. (See table II.) No loss in load nor increase in strain near the point of impact was detected. This panel was subsequently loaded to an applied strain of 0.0062 at which a moiré-fringe pattern was observed in the end regions (see fig. 13) similar to that observed for the undamaged test panel. A local fringe pattern can be seen in the figure at each impact location.

Following this test the panel was inspected ultrasonically to evaluate the extent of the damaged region. The subsurface-damage region is outlined on the panel in figure 13. The two damaged regions are about the same size, which indicates that the magnitude of the applied strain had no apparent effect on the extent of local damage. These results indicate that impact damage in the regions having high axial stiffness is significantly more detrimental than it is in regions of low axial stiffness.

CONCLUDING REMARKS

An exploratory investigation was conducted to determine the effect of low-velocity impact damage on the compression strength of graphite-epoxy hat-stiffened panels. Fourteen panels were tested in this investigation and the results indicate that low-velocity impact, typical of that which may be inflicted by runway debris, can have a significant effect on panel compression strength. Runway-debris hazards were simulated in this study by 1.27-cm-diameter aluminum spheres impacting at velocities around 55 m/s. High- and low-axial-stiffness regions of the panel cross sections were subjected to impact. The impacting sphere caused local damage in both regions. Damage in the low-axial-stiffness region was found to have little effect on panel strength. Damage in the high-axial-stiffness region of panels designed for 1.58 MN/m at a strain of 0.0080 caused these panels to fail at applied axial strains 50 to 58 percent of the design level. Damage in the high-axial-

stiffness regions of panels designed for 0.53 MN/m at a strain of 0.0034 was contained locally and these panels were capable of carrying the design load.

The extent of local damage induced by impact in regions of high axial stiffness was found to increase with the magnitude of applied axial-compression strain present at impact. The existence of, and not necessarily the extent of, local damage was found to be the significant factor in reducing the strength of panels designed for 1.58 MN/m. Limited local damage that was not visually detectable (but which could be identified by ultrasonic inspection) reduced the ultimate strength as much as extensive visible damage. Impact caused considerable delamination and the discrete layers thus formed can exhibit anisotropic effects. Such delamination also introduces local eccentric forces in the panel that develop high normal and shear stresses at the boundary of the delaminated region, and these delaminated regions can buckle locally at reduced applied loads. These effects could contribute to local load redistribution in the panel and cause the damage to propagate.

A panel designed for 1.58 MN/m was tested to failure with a 1.27-cm-diameter cutout in the region of high axial stiffness to provide comparative data for a panel with a well-defined flaw. Two types of local failure were observed near the cutout. First, localized material failure occurred at the cutout boundary. Second, local buckling in the region of the cutout was observed prior to failure. The local buckling subsequently precipitated panel failure at 73 percent of the design strain level. This strength reduction was not as severe as that caused by impact damage; however, the cutout was smaller than the impact-damaged areas.

The results of this exploratory investigation suggest that highly efficient graphite-epoxy hat-stiffened compression panels designed for a 0.0080 strain level can exhibit serious compressive strength degradation due to low-velocity impact damage. However, panels designed for more moderate strains (0.0034, for example) are not degraded by such impacts even in regions of high axial stiffness.

Langley Research Center
National Aeronautics and Space Administration
Hampton, VA 23665
February 7, 1977

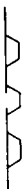







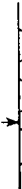
REFERENCES

1. Williams, Jerry G.; and Mikulas, Martin M., Jr.: Analytical and Experimental Study of Structurally Efficient Composite Hat-Stiffened Panels Loaded in Axial Compression. AIAA Paper No. 75-754, May 1975.
2. Williams, Jerry G.; and Stein, Manuel: Buckling Behavior and Structural Efficiency of Open-Section Stiffened Composite Compression Panels. AIAA Paper 76-1727, May 1976.
3. Rhodes, Marvin D.: Impact Fracture of Composite Sandwich Structures. AIAA Paper 75-748, May 1975.
4. Mikulas, Martin M., Jr.; Bush, Harold G.; and Rhodes, Marvin D.: Current Langley Research Center Studies on Buckling and Low Velocity Impact of Composite Panels. Third Conference on Fibrous Composites in Flight Vehicle Design, Part II, NASA TM X-3377, 1976, pp. 633-663.
5. Agarwal, Banarsi; and Davis, Randall C.: Minimum-Weight Designs for Hat-Stiffened Composite Panels Under Uniaxial Compression. NASA TN D-7779, 1974.
6. Platt, Robert J., Jr.; and Thurston, Lewis B., Jr.: Holographic and Ultrasonic Detection of Bond Flaws in Aluminum Panels Reinforced With Boron-Epoxy. NASA TN D-7632, 1974.

TABLE I.- ELASTIC MATERIAL PROPERTIES USED IN PANEL DESIGNS

Longitudinal modulus, GN/m ² (lbf/in ²)	131 (19.0 × 10 ⁶)
Transverse modulus, GN/m ² (lbf/in ²)	13.0 (1.89 × 10 ⁶)
Shear modulus, GN/m ² (lbf/in ²)	6.41 (0.93 × 10 ⁶)
Major Poisson's ratio	0.38
Density, g/cm ³ (lbm/in ³)	1.52 (0.055)
Ply thickness, mm (in.)	0.14 (0.0055)

TABLE II.- TEST CONDITIONS AND RESULTS

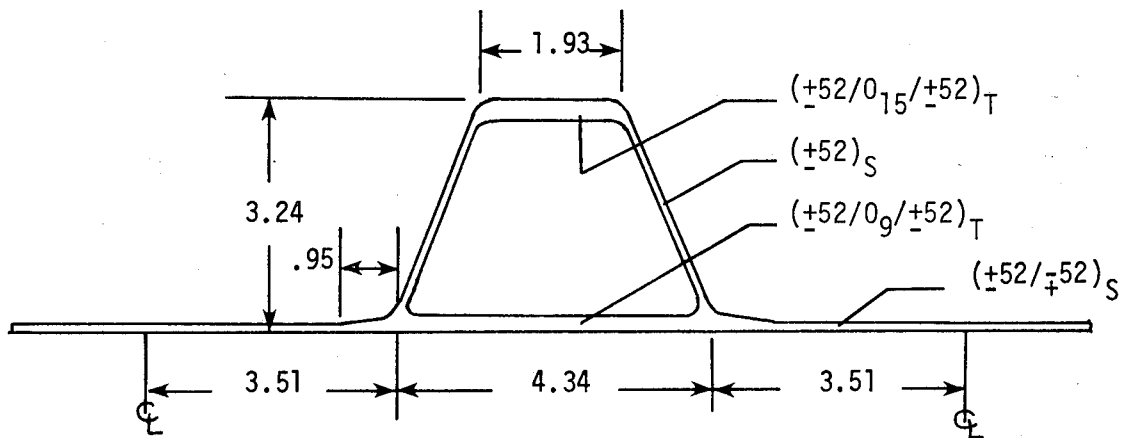
Test	Panel data			Load condition data				Cutout and impact test data				Residual strength			
	No.	Length, cm	Width, cm	ϵ_a	* ϵ_a/ϵ_D	Load, kN	Response	Velocity, m/s	Location	Load after impact, kN	Subsurface damage size†	ϵ_a	ϵ_a/ϵ_D	Load, kN	
Control	Undamaged panels	Design A	A1	40.4	17.8	0.0032	0.94	100	Buckled						
			A2	40.4	17.8	0.0035	1.03	107	Buckled						
			A3	43.7	28.7	0.0037	1.09	162	Buckled						
			B1	40.6	22.1	0.0072	0.90	402	Ultimate						
		Design B	B2	40.6	22.1	0.0080	1.00	443	Ultimate						
			B3	40.6	22.1	0.0082	1.03	453	Ultimate						
			B4	40.6	22.1	0.0082	1.03	453	Ultimate						
			B5	40.6	36.8										0.0058
Impact damage	Damage in high-axial-stiffness region	Low axial load	A4	43.7	28.7	0	0	0	53.9		0	Width of hat base by 6.4 cm long	0.0036	1.05	166
			A5	43.7	40.1	0	0	0	51.5		0	Width of hat cap by 3.6 cm long	0.0034	1.00	197
			B6	40.6	36.8	0.0003	0.04	22.2	50.6		22.2	2.5 cm wide by 3.8 cm long	0.0043	0.54	374
			†A3	43.7	28.7	0.0034	1.00	148	50.9		129	14.0 cm by 14.0 cm	0.0037	1.09	140
		High axial load	B7	40.6	36.8	0.0030	0.38	258	53.3		229	No data available	0.0046	0.58	345
			B8	40.6	36.8	0.0040	0.50	351	57.9		0	Catastrophic failure on impact			
			†B9	40.6	36.8	0.0040	0.51	347	52.4		347	2.8-cm-diameter circle with 5.1- to 6.4-cm spike at 450			
												467		0.0062	0.78

*Applied axial strain ϵ_a ; design axial strain ϵ_D .

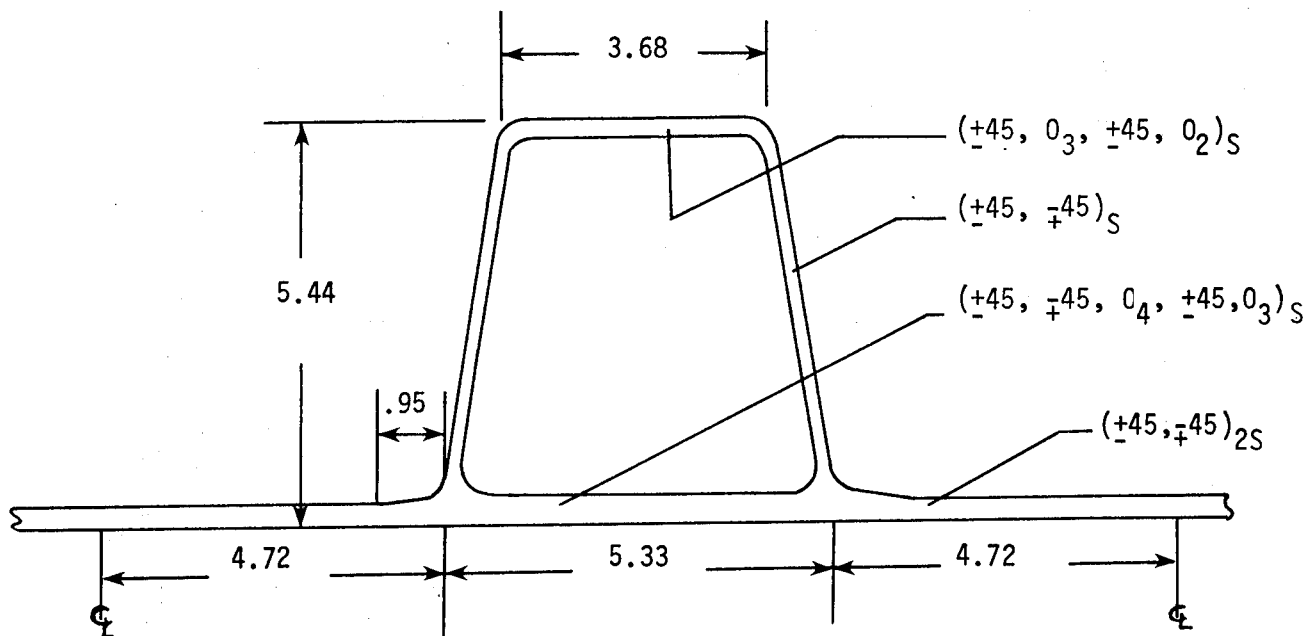
†Estimate based on ultrasonic test.

‡Specimen used for multiple tests.

#Loading stopped, did not fail.



(a) Design A. Axial strain equals 0.0034 at applied design load of 0.53 MN/m. Axial stiffness (EA) of typical repeating element is 16.5 MN.



(b) Design B. Axial strain equals 0.0080 at applied design load of 1.58 MN/m. Axial stiffness (EA) of typical repeating element is 31.7 MN.

Figure 1.- Design details of typical stiffener cross sections (dimensions in cm).

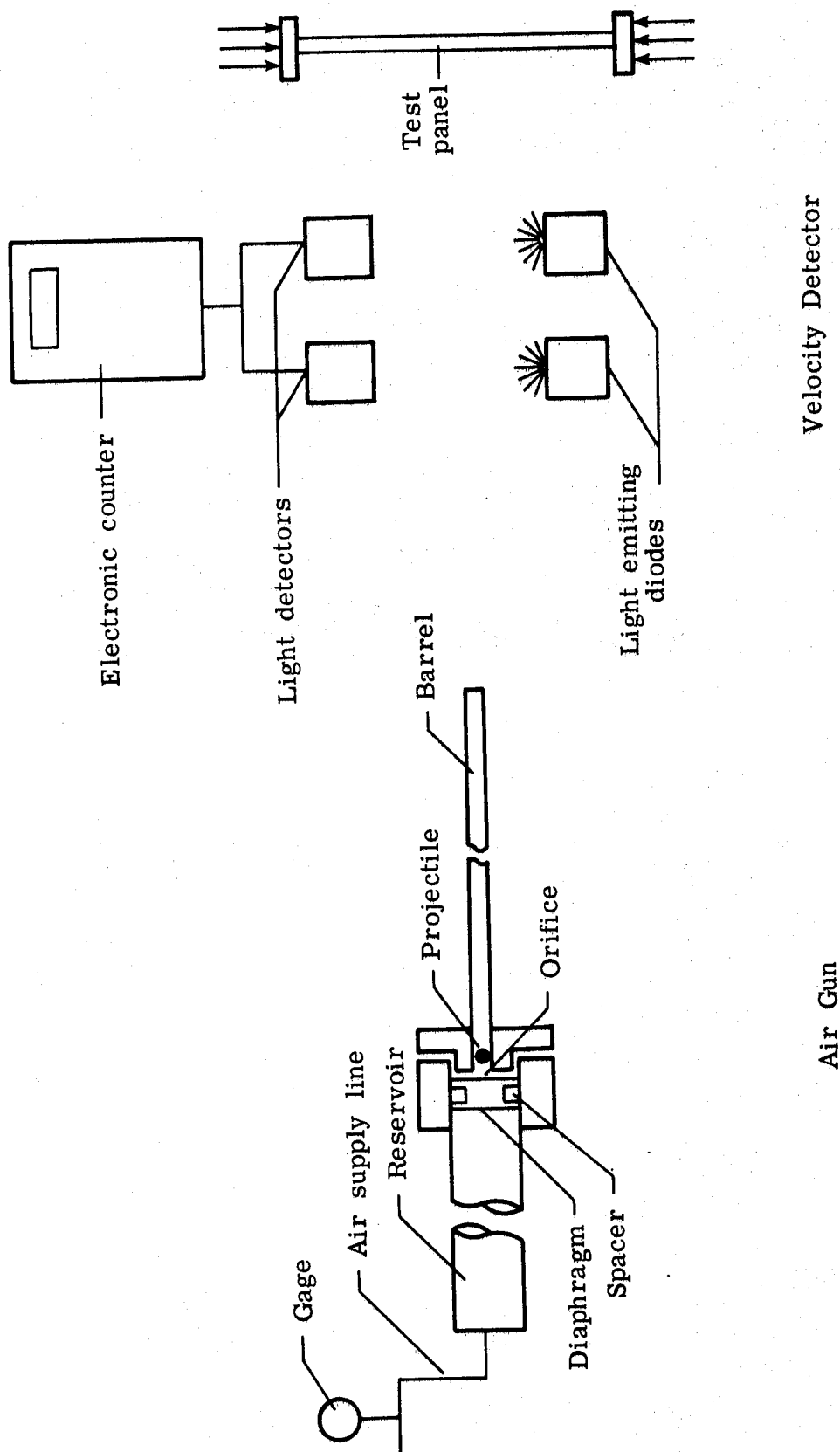
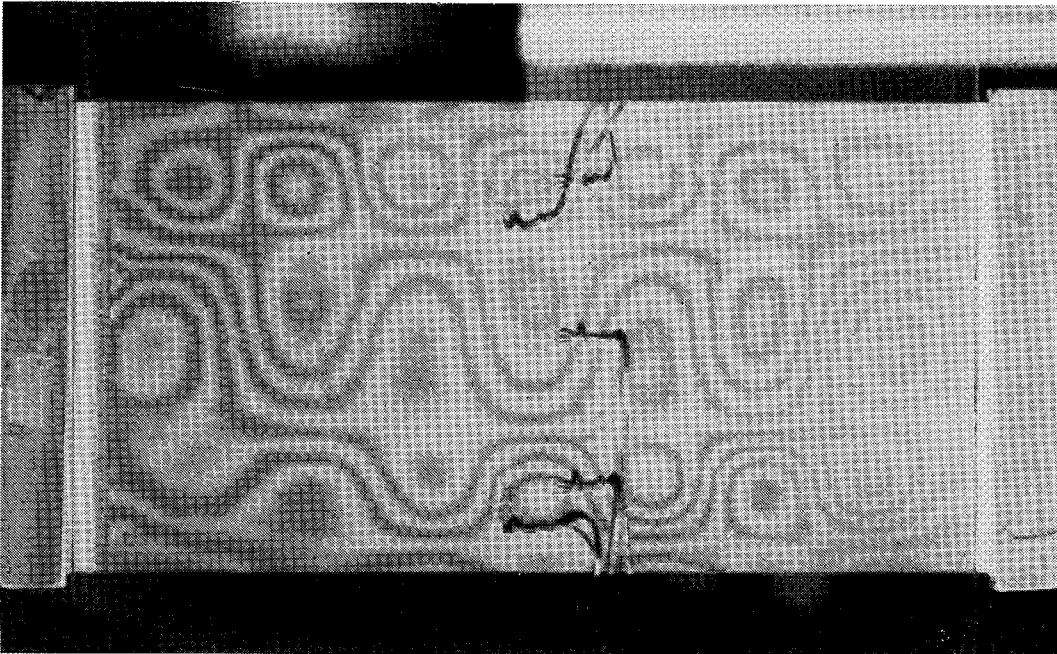
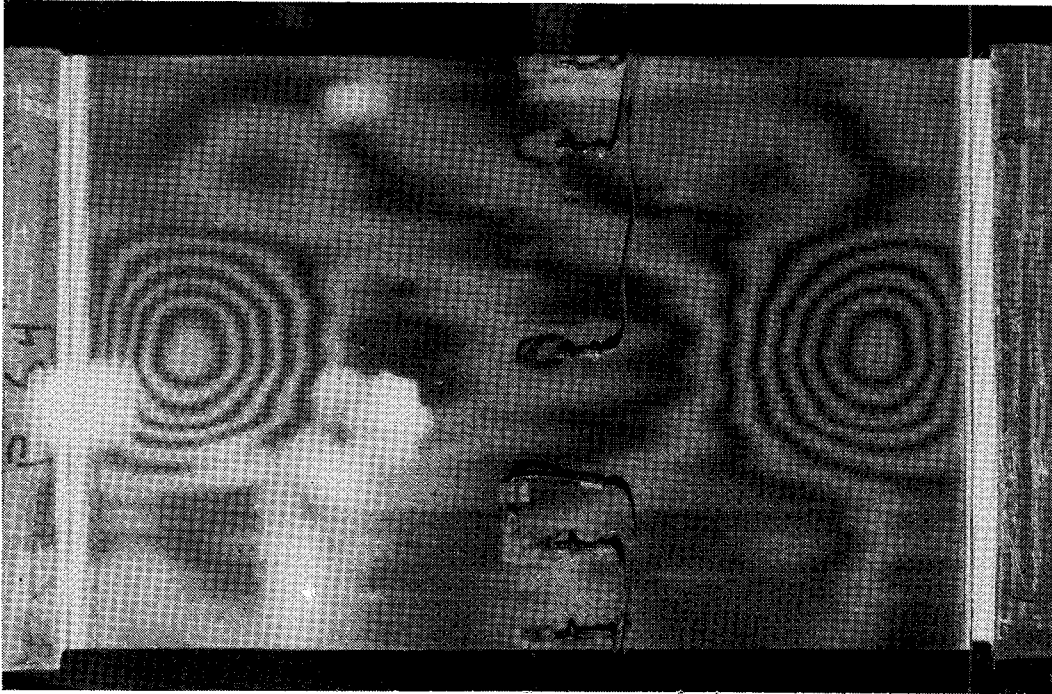


Figure 2.- Schematic drawing of air gun and velocity detector.



(a) Panel A1 designed for strain of 0.0034
loaded to strain of 0.0036.



(b) Panel B2 designed for strain of 0.0080
loaded to strain of 0.0079.

L-77-142

Figure 3.- Photographs of moiré-fringe patterns for typical undamaged panels
during compression tests.

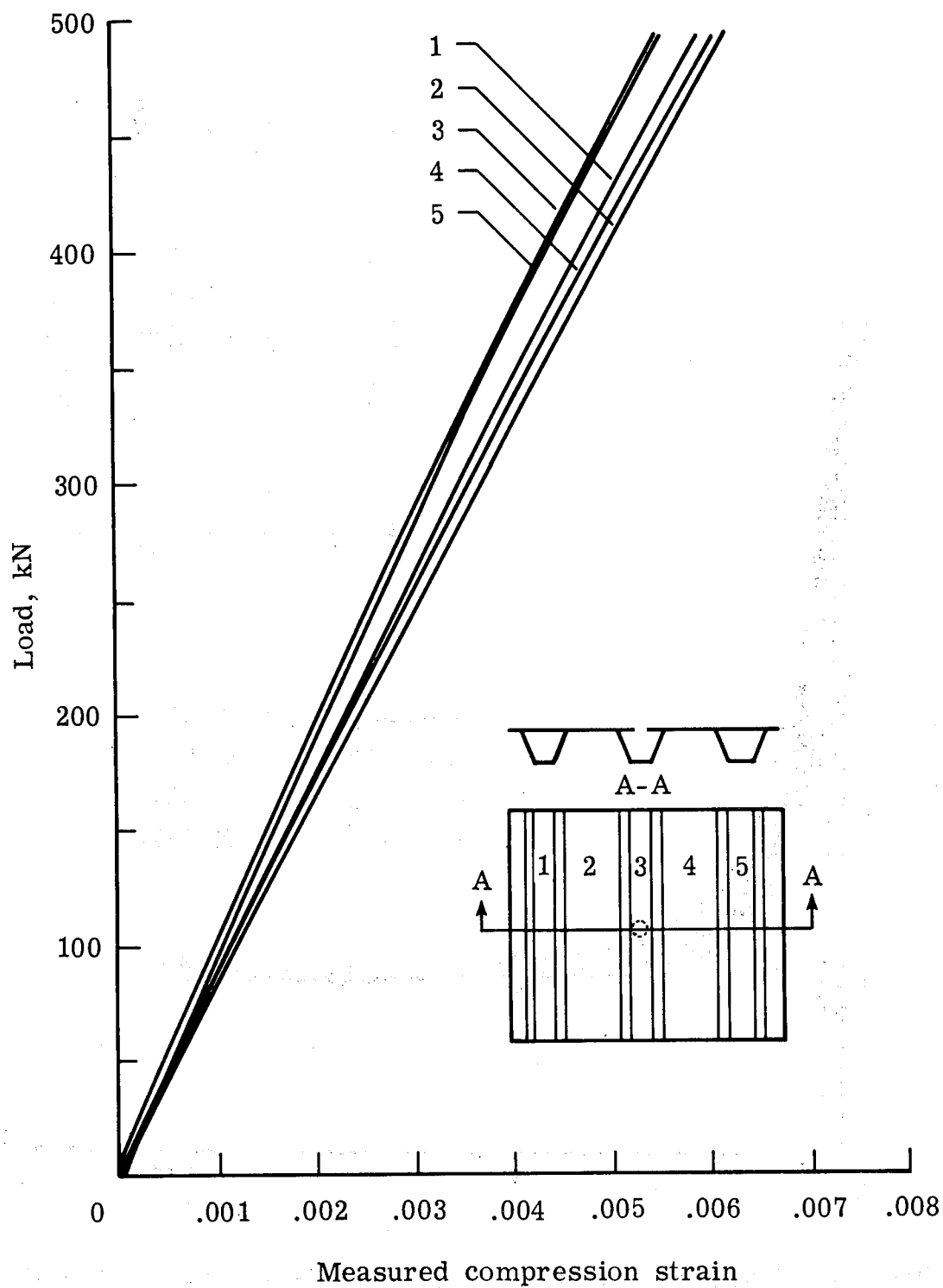


Figure 4.- Compression load-strain curves at five locations across panel B5 which has 1.27-cm-diameter cutout in high-axial-stiffness region of center stiffener.

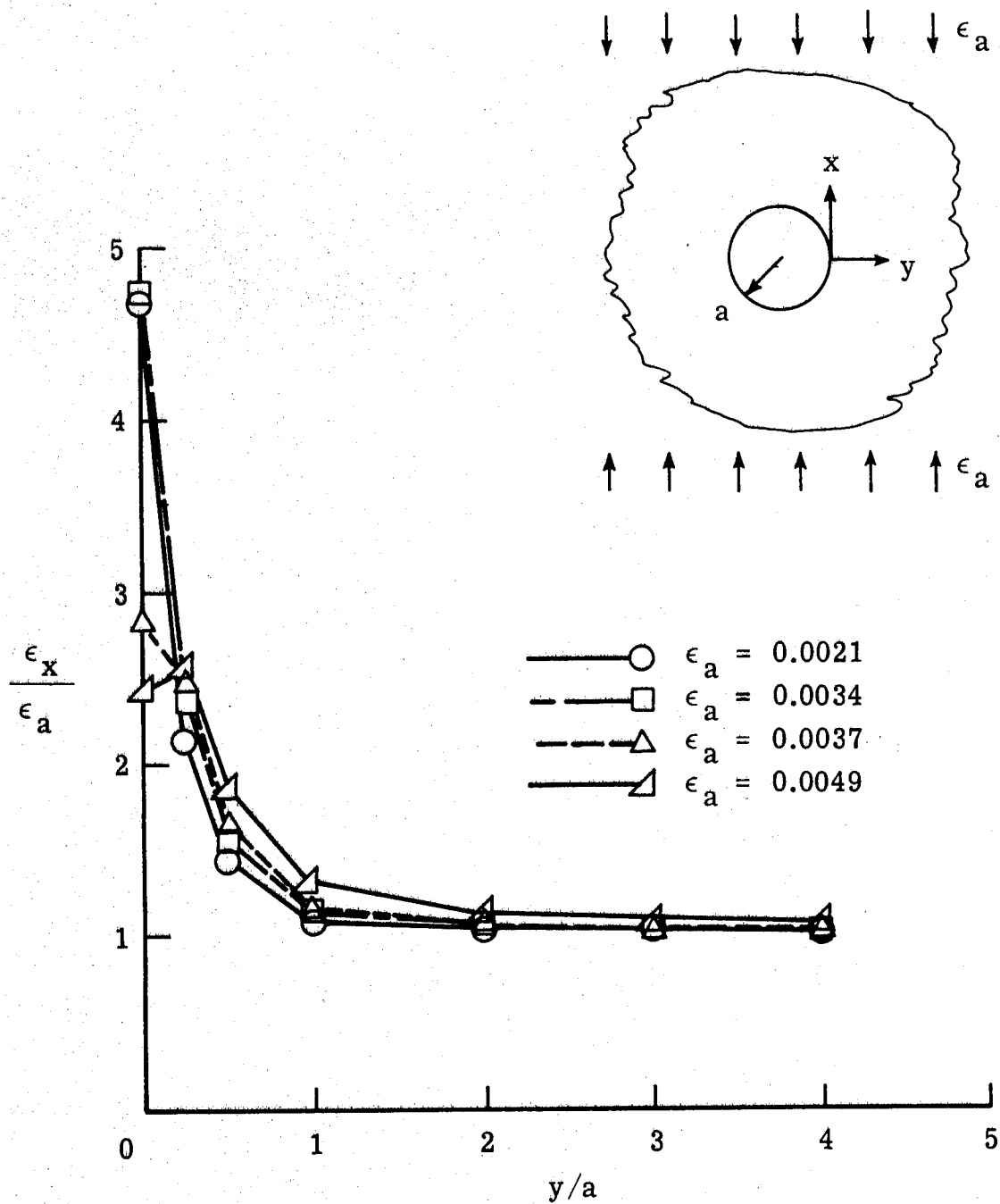
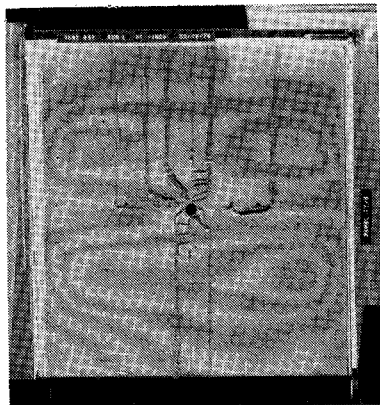


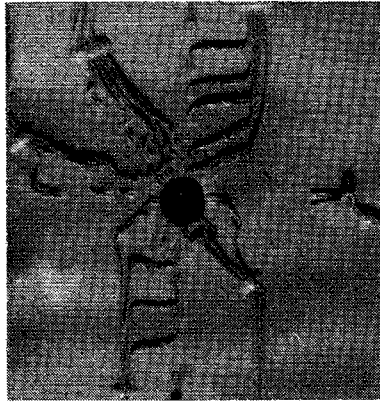
Figure 5.- Strain measured in vicinity of 1.27-cm-diameter cutout on panel B5 (ϵ_x denotes measured strain at indicated location at applied axial strain ϵ_a).



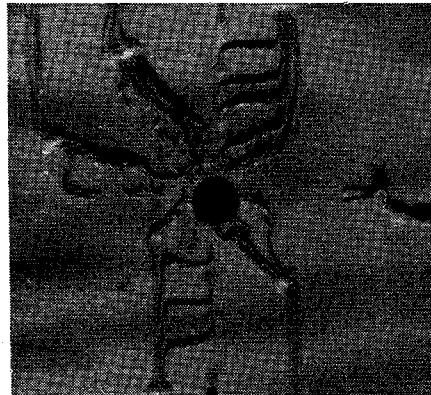
(a) $\epsilon_a = 0.0048$.



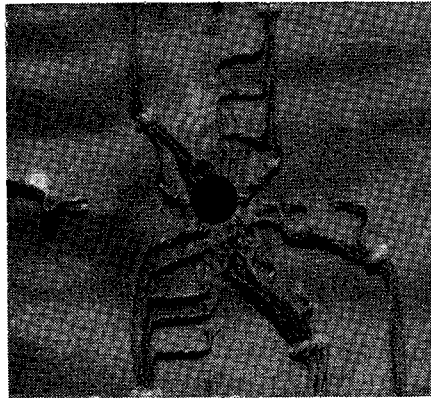
(b) $\epsilon_a = 0.0048$.



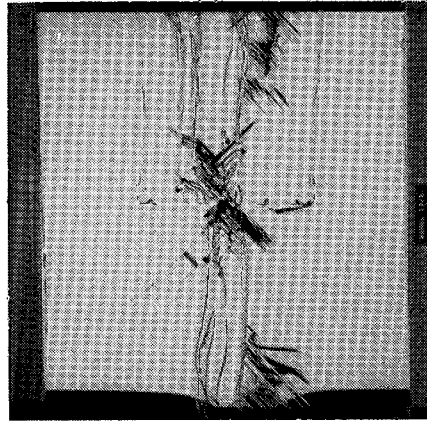
(c) $\epsilon_a = 0.0050$.



(d) $\epsilon_a = 0.0055$.

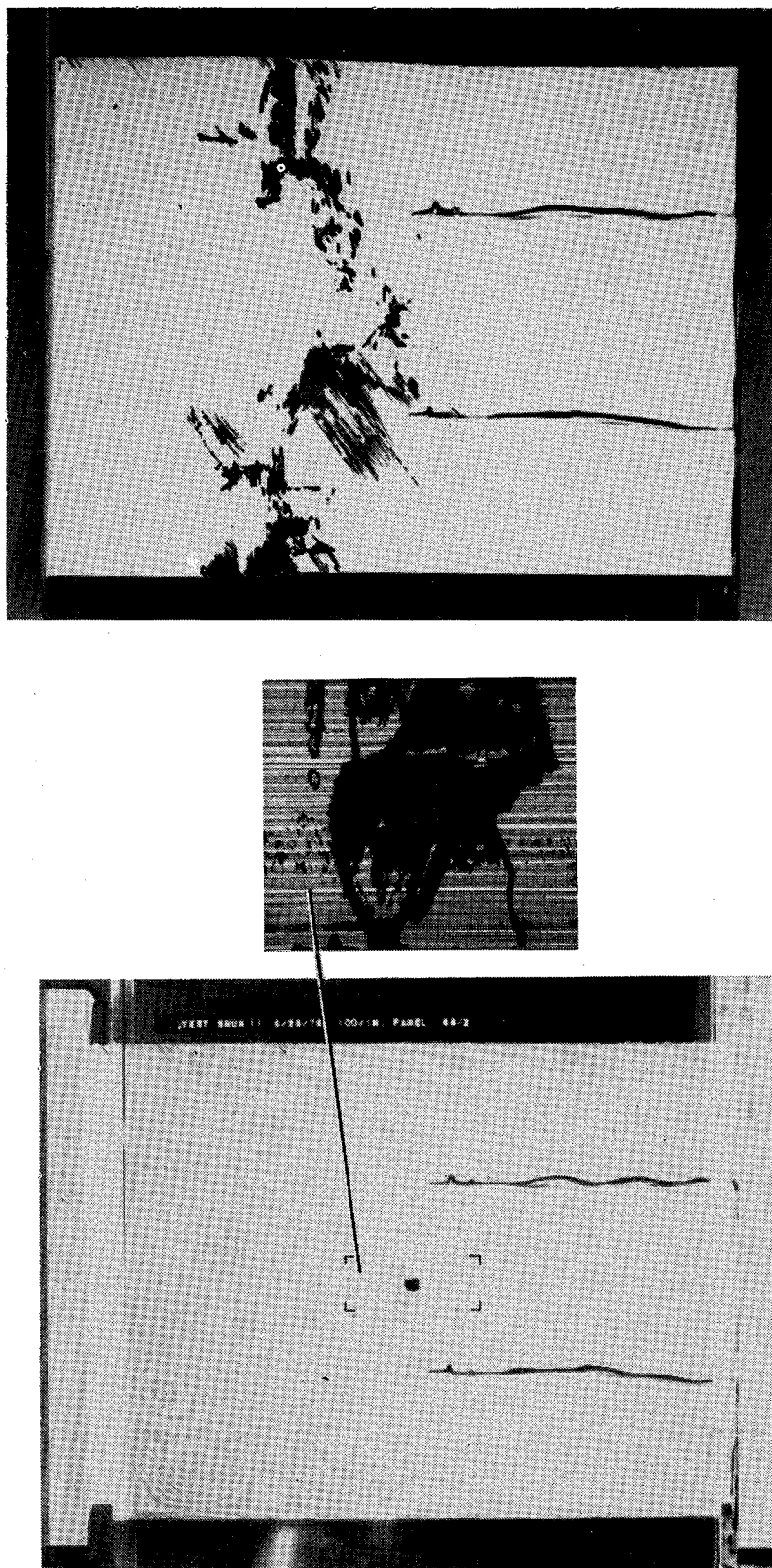


(e) $\epsilon_a = 0.0057$.



(f) $\epsilon_a = 0.0058$.

Figure 6.- Photographs of moiré-fringe patterns of panel B5 at several values of applied axial strain ϵ_a .
L-77-143

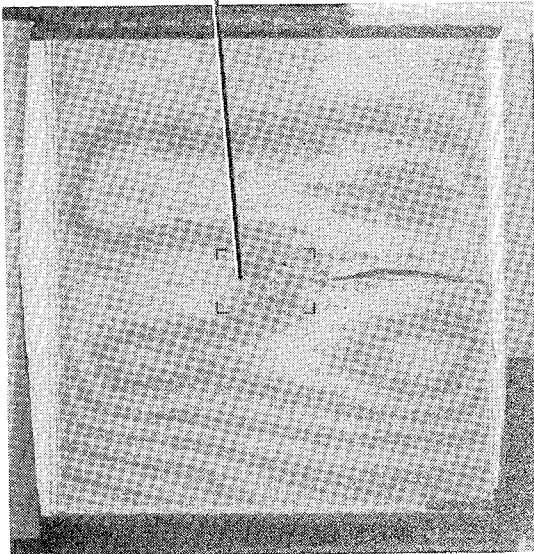


(a) Photograph of moiré-fringe pattern of buckled panel at applied axial strain of 0.0035. Insert shows region of subsurface damage.

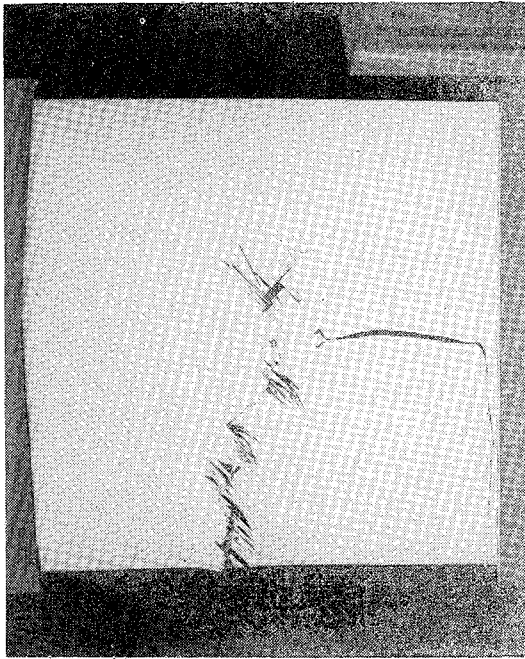
(b) Panel after failure.

Figure 7.- Panel A4 (after impact in high-axial-stiffness region while at zero applied axial strain) before and after failure.

L-77-144



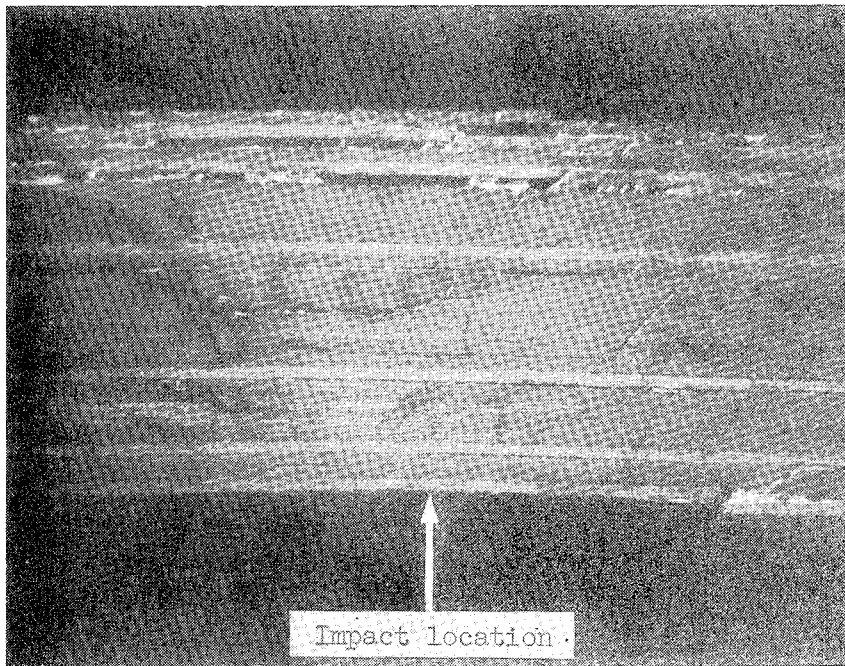
(a) Photograph of moiré-fringe pattern at applied axial strain of 0.0041 showing development of fringe pattern near point of impact. Insert shows region typical of subsurface damage in similar test panel.



(b) Panel after failure.

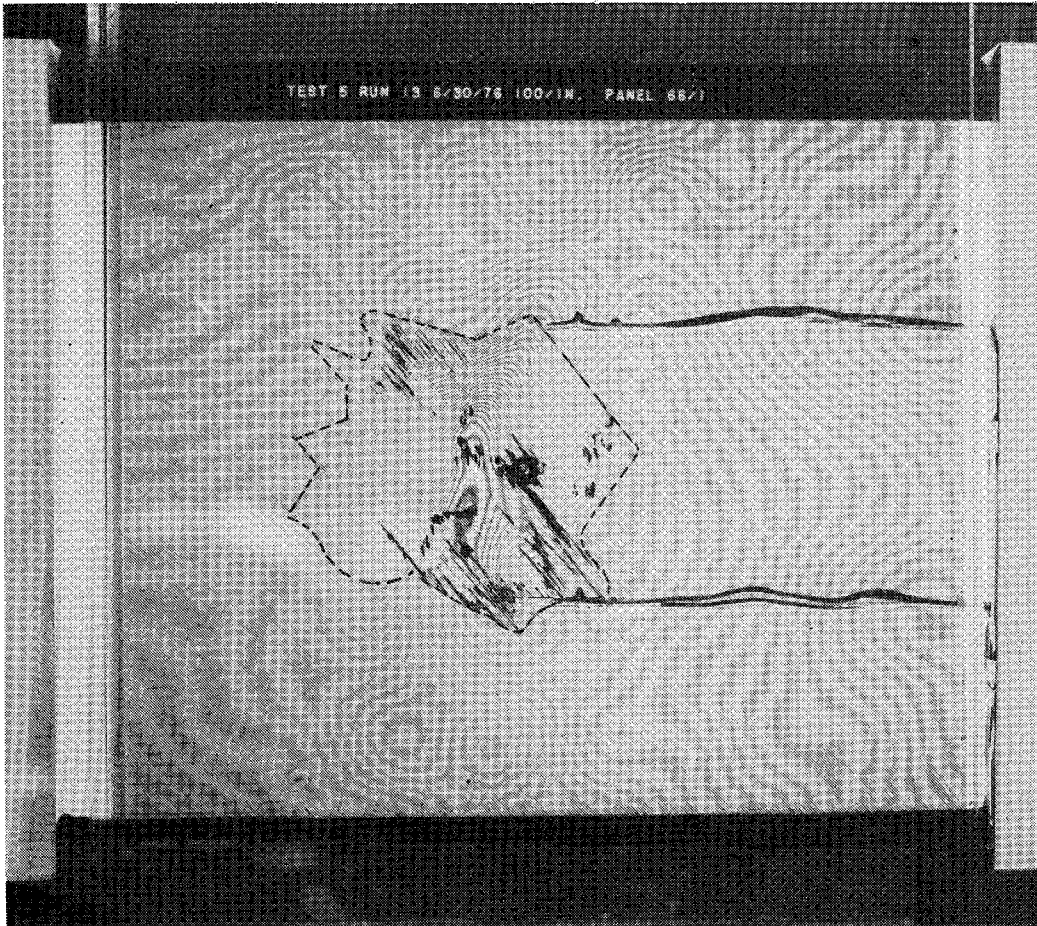
Figure 8.- Panel B6 (after impact in high-axial-stiffness region while at applied strain of 0.0003) before and after failure.

L-77-145

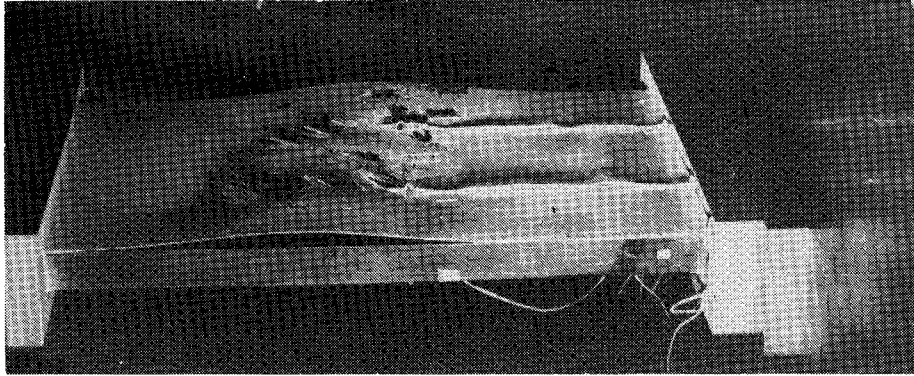


L-77-146

Figure 9.- Photomicrograph of cross section of high-axial-stiffness region of panel similar to B6 after being subjected to impact damage at zero applied axial strain.



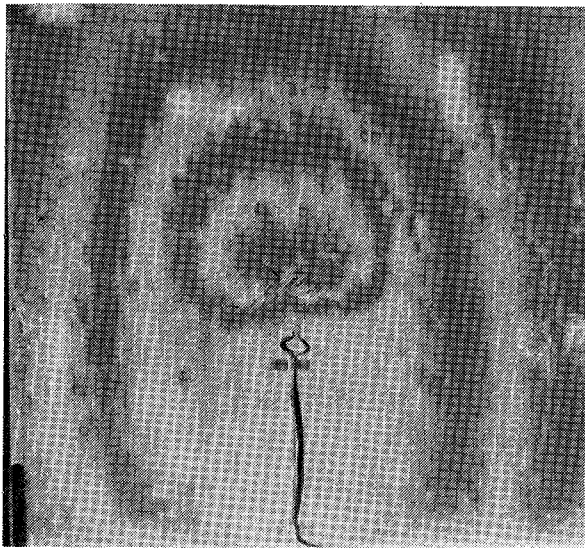
(a) Photograph of moiré-fringe pattern of buckled panel at applied axial strain of 0.0031.



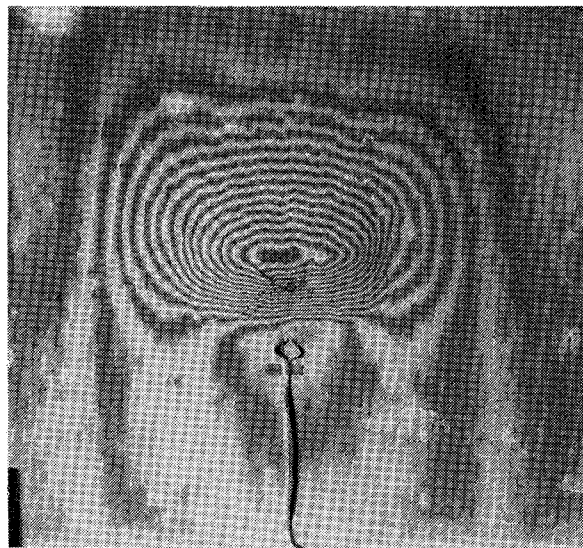
(b) Panel after failure.

L-77-147

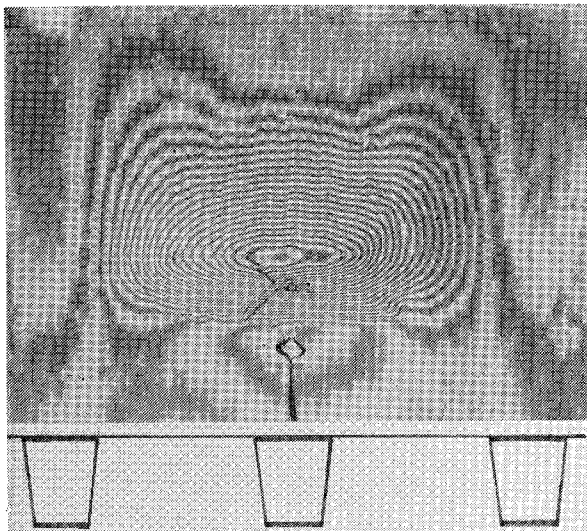
Figure 10.- Panel A3 (after impact in high-axial-stiffness region while at applied strain of 0.0034) before and after failure.



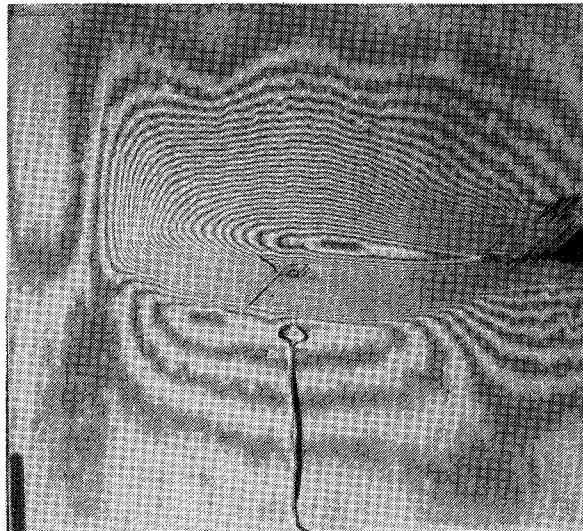
(a) Panel with zero applied strain.



(b) Panel at applied strain of 0.0021.



(c) Panel at applied strain of 0.0043.



(d) Panel after failure.

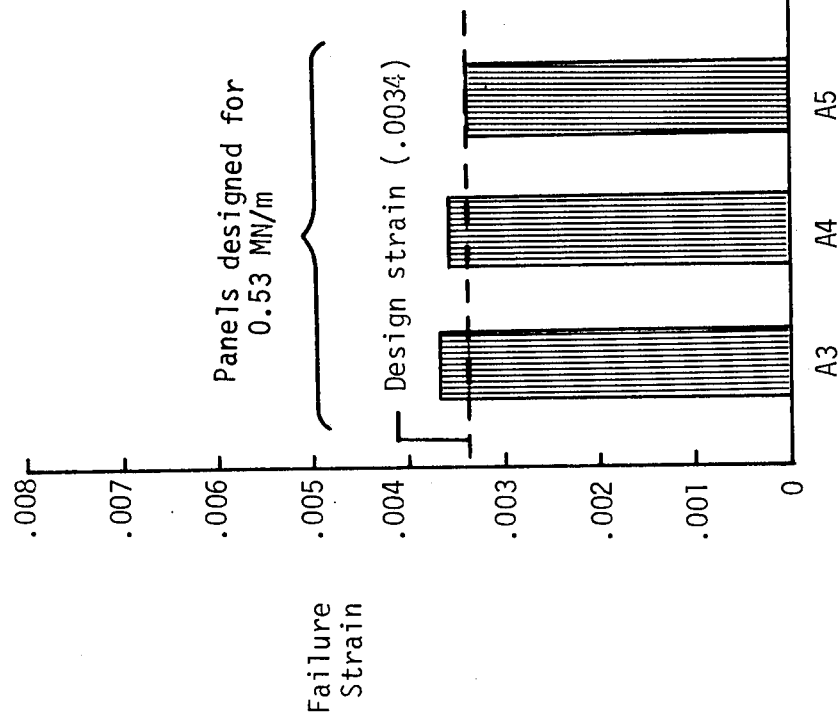
Figure 11.- Panel B7 (after impact in high-axial-stiffness region while at applied strain of 0.0030) before and after failure.

L-77-148

Panels designed for 1.58 MN/m

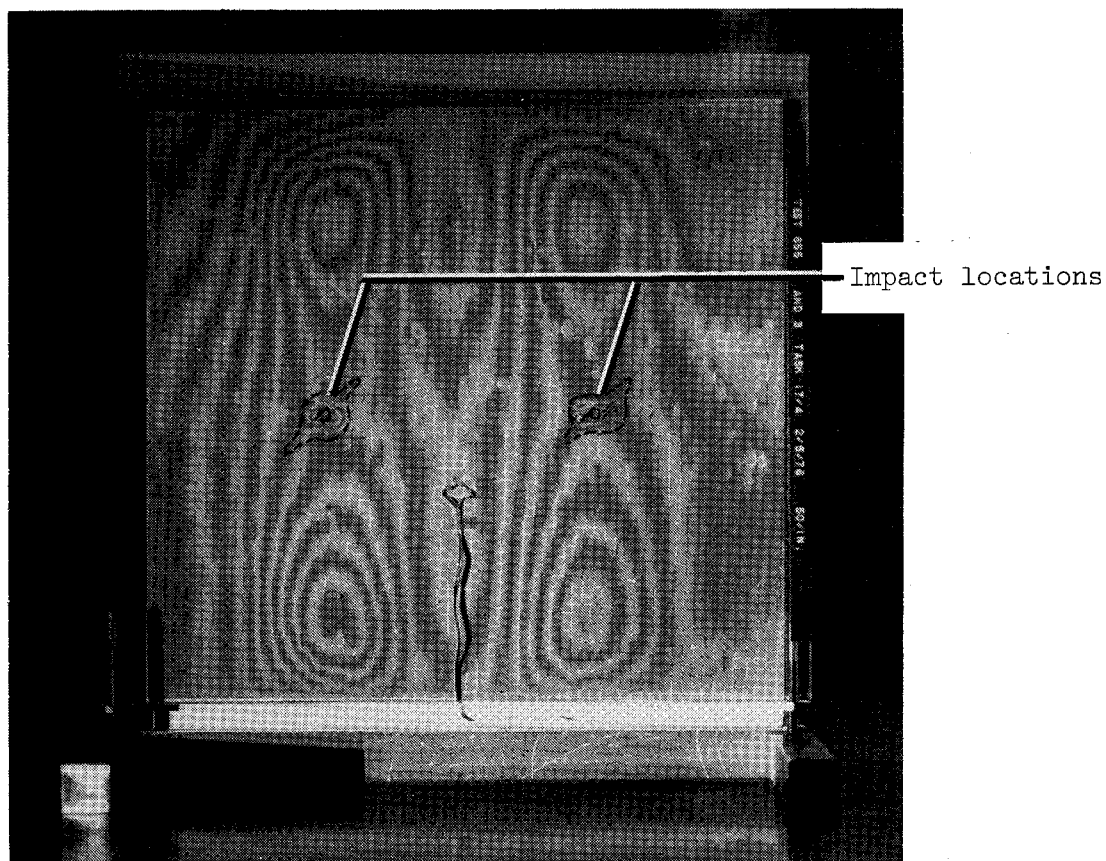
Z-----
Design strain (.0080)

Control panel with 1.27-cm-diameter cutout



Panel

Figure 12.- Failure strains for panels damaged by impact in high-axial-stiffness region and for control panel.



L-77-149
Figure 13.- Photograph of moiré-fringe pattern for panel B9 at applied axial strain of 0.0062 with impact damage at two locations in low-axial-stiffness region.

NATIONAL AERONAUTICS AND SPACE ADMINISTRATION
WASHINGTON, D.C. 20546

OFFICIAL BUSINESS
PENALTY FOR PRIVATE USE \$300

SPECIAL FOURTH-CLASS RATE
BOOK

POSTAGE AND FEES PAID
NATIONAL AERONAUTICS AND
SPACE ADMINISTRATION
451



259 001 C1 U D 770401 S00942DS
DEPT OF THE ARMY
PICATINNY ARSENAL, BLDG 176
PLASTICS TECHNICAL EVALUATION CENTER
ATTN: A M ANZALONE, SARPA-FR-M-D
DOVER NJ 07801

3401

If Undeliverable (Section 158
Postal Manual) Do Not Return

"The aeronautical and space activities of the United States shall be conducted so as to contribute . . . to the expansion of human knowledge of phenomena in the atmosphere and space. The Administration shall provide for the widest practicable and appropriate dissemination of information concerning its activities and the results thereof."

—NATIONAL AERONAUTICS AND SPACE ACT OF 1958

NASA SCIENTIFIC AND TECHNICAL PUBLICATIONS

TECHNICAL REPORTS: Scientific and technical information considered important, complete, and a lasting contribution to existing knowledge.

TECHNICAL NOTES: Information less broad in scope but nevertheless of importance as a contribution to existing knowledge.

TECHNICAL MEMORANDUMS: Information receiving limited distribution because of preliminary data, security classification, or other reasons. Also includes conference proceedings with either limited or unlimited distribution.

CONTRACTOR REPORTS: Scientific and technical information generated under a NASA contract or grant and considered an important contribution to existing knowledge.

TECHNICAL TRANSLATIONS: Information published in a foreign language considered to merit NASA distribution in English.

SPECIAL PUBLICATIONS: Information derived from or of value to NASA activities. Publications include final reports of major projects, monographs, data compilations, handbooks, sourcebooks, and special bibliographies.

TECHNOLOGY UTILIZATION PUBLICATIONS: Information on technology used by NASA that may be of particular interest in commercial and other non-aerospace applications. Publications include Tech Briefs, Technology Utilization Reports and Technology Surveys.

Details on the availability of these publications may be obtained from:

SCIENTIFIC AND TECHNICAL INFORMATION OFFICE

NATIONAL AERONAUTICS AND SPACE ADMINISTRATION

Washington, D.C. 20546